The Meteoritical Society

Meteoritics & Planetary Science 41, Nr 12, 1883–1898 (2006)
Abstract available online at http://meteoritics.org

Estimating shock pressures based on high-pressure minerals in shock-induced melt veins of L chondrites

Zhidong XIE[1*], Thomas G. SHARP[1], and Paul S. DE CARLI[2]

[1]School of Earth and Space Exploration, Arizona State University, Tempe, Arizona 85287, USA
[2]SRI International, 333 Ravenswood Avenue, Menlo Park, California 94025, USA
[*]Corresponding author. E-mail: zhidong.xie@asu.edu

(Received 24 April 2006; revision accepted 24 September 2006)

Abstract–Here we report the transmission electron microscopy (TEM) observations of the mineral assemblages and textures in shock-induced melt veins from seven L chondrites of shock stages ranging from S3 to S6. The mineral assemblages combined with phase equilibrium data are used to constrain the crystallization pressures, which can be used to constrain shock pressure in some cases. Thick melt veins in the Tenham L6 chondrite contain majorite and magnesiowüstite in the center, and ringwoodite, akimotoite, vitrified silicate-perovskite, and majorite in the edge of the vein, indicating crystallization pressure of ~25 GPa. However, very thin melt veins (5–30 μm wide) in Tenham contain glass, olivine, clinopyroxene, and ringwoodite, suggesting crystallization during transient low-pressure excursions as the shock pressure equilibrated to a continuum level. Melt veins of Umbarger include ringwoodite, akimotoite, and clinopyroxene in the vein matrix, and Fe_2SiO_4-spinel and stishovite in SiO_2-FeO-rich melt, indicating a crystallization pressure of ~18 GPa. The silicate melt veins in Roy contain majorite plus ringwoodite, indicating pressure of ~20 GPa. Melt veins of Ramsdorf and Nakhon Pathon contain olivine and clinoenstatite, indicating pressure of less than 15 GPa. Melt veins of Kunashak and La Lande include albite and olivine, indicating crystallization at less than 2.5 GPa. Based upon the assemblages observed, crystallization of shock veins can occur before, during, or after pressure release. When the assemblage consists of high-pressure minerals and that assemblage is constant across a larger melt vein or pocket, the crystallization pressure represents the equilibrium shock pressure.

INTRODUCTION

Shock metamorphism, resulting from hypervelocity collision, is one of the most fundamental processes in the solar system (Chao 1967; Stöffler 1972; Kieffer 1975; Stöffler et al. 1991; Bischoff and Stöffler 1992; Chen et al. 1996; Sharp et al. 1997; Langenhorst and Poirier 2000; Leroux 2001). Shock metamorphism includes brecciation, deformation, local melting, recrystallization, and phase transformation. This study focuses on the high-pressure phases that crystallize from silicate melt in shock-induced melt veins.

Early studies of shock metamorphism concentrated on terrestrial samples that contained high-pressure silicates such as coesite and stishovite (Chao et al. 1960; Chao et al. 1962; Chao 1967; Shoemaker and Chao 1961). Shock deformation features in meteorites were studied intensively by optical microscopy and X-ray diffraction in the late 1960s (Milton and De Carli 1963; Fredriksson et al. 1963; Van Schmus and Wood 1967; Heymann 1967; Carter et al. 1968; Van Schmus and Ribbe 1968; Taylor and Heymann 1969; Stöffler 1972, 1974). Since the late 1970s, shock-induced deformation microstructures such as planar deformation features (PDF), twinning, and plastic deformation have been studied intensively using transmission electron microscopy (TEM) (Price et al. 1979; Ashworth 1985; Goltrant et al. 1991; Goltrant et al. 1992; Cordier and Gratz 1995; Langenhorst et al. 1995; Leroux 2001). The main goal of these studies was to constrain shock conditions (pressure, temperature, and time) based on shock effects in shocked chondrites. This required a pressure calibration for the deformation and transformation process that occur during shock.

The widely used shock classification scheme and pressure calibration for chondrites by Stöffler et al. (1991) is based on the comparison of deformation and transformation effects between natural and experimentally shocked samples. Based on shock effects in olivine and plagioclase as recognized by petrographic analysis of thin sections, six stages of shock (S1 to S6) are defined. Calibration of shock

effects provides pressure estimates for the shock-stage transitions S1/S2, S2/S3, S3/S4, S4/S5, S5/S6, and whole rock melting at <5, 5–10, 15–20, 30–35, 45–55, and 75–90 GPa, respectively (Stöffler et al. 1991). This shock classification system is easy to apply and correctly represents the progressive shock-metamorphic sequence from weak to strong. However, pressure calibration based on microsecond-duration shock-recovery experiments is problematic for shock features that depend on reaction kinetics, such as phase transformations (De Carli et al. 2002; Sharp and De Carli 2006). Silicate phase transformations that occur during shock are generally reconstructive and are strongly dependent on time and temperature as well as pressure.

Recently, an alternative means of estimating shock pressure has been used. This approach uses the mineralogy of melt veins to estimate crystallization conditions based on phase relations determined in static high-pressure experiments (Chen et al. 1996; Sharp et al. 1997; Tomioka and Fujino 1997; Gillet et al. 2000; Chen et al. 2003; Chen et al. 2004a; Xie and Sharp 2004; Beck et al. 2005; Xie et al. 2006). Close similarities in mineralogy, grain size, composition, and microstructure between the samples from static experiments and melt-vein material in the Sixiangkou (Chen et al. 1996), Acfer 040 (Sharp et al. 1997), Tenham (Tomioka and Fujino 1997; Xie et al. 2006), Umbarger (Xie et al. 2002), and other heavily shocked L6 chondrites suggest that the results of static high-pressure experiments can be used to estimate or constrain the conditions of melt-vein crystallization. However, all of these studies have involved heavily shocked S6 samples that have abundant high-pressure minerals. The purpose of this study is to determine melt-vein crystallization conditions in samples of variable shock stage (S3–S6) and explore the relationship between melt-vein crystallization pressure and shock pressure.

The shock-induced origin of melt veins in chondrites was demonstrated by Fredricksson et al. (1963), who synthesized black veins in shock experiments. Melt veins have been described as "polymict breccias" (Reichenbach 1860), "shock-induced veins" (Fredriksson et al. 1963), "shock blackening veins" (Heymann 1967), "polymineralic mixed melts" (Dodd and Jarosewich 1979), and "shock-induced localized melting" (Stöffler et al. 1991). Shock-induced melt veins commonly contain two lithologies. One consists of polycrystalline grains that transformed from host rock fragments by solid-state polymorphic phase transitions (Chen et al. 1996). The other consists of quenched silicate and metal-sulfide that crystallized from shock-induced melts (Chen et al. 1996). In highly shocked (S6) meteorites, both lithologies commonly contain high-pressure minerals, similar to those expected in the Earth's transition zone (410–660 km in depth) and lower mantle (>660 km in depth). These minerals include wadsleyite, ringwoodite, majorite, akimotoite, silicate perovskite, hollandite-structured plagioclase, post-stishovite SiO_2 polymorphs, and Fe_2SiO_4-spinel (Mason et al. 1968; Binns et al. 1969; Putnis and Price 1979; Price et al. 1979; Price et al. 1982; Sharp et al. 1997; Tomioka and Fujino 1997; El Goresy et al. 2000; Sharp et al. 1999; Gillet et al. 2000; Langenhorst and Poirier 2000; Xie et al. 2002; Chen et al. 2004a; Xie and Sharp 2004; Xie et al. 2006). The high-pressure minerals in the shock-induced melt veins of meteorites not only provide high-pressure indicators for the shock event, they also provide natural samples of deep Earth materials that are not found in terrestrial rocks.

There are relatively few studies of the mineralogy of shock-induced melt veins in chondrites of shock stages S3 to S5 (Xie and Sharp 2000; Xie et al. 2002). The melt veins in highly shocked chondrites (shock grade S6) have been extensively studied because these samples contain important high-pressure minerals such as ringwoodite, majorite, and wadsleyite (Mason et al. 1968; Binns et al. 1969; Putnis and Price 1979; Price et al. 1979), which are often used as indicators of the S6 shock grade. Melt veins in samples of shock grades S3 to S5 are generally regarded as a subordinate indicator of shock grade.

Here we present detailed observations of the microtextures and mineral assemblages in shock-induced melt veins in samples ranging from shock stage S3 to S6. The purpose of this study is to determine how melt-vein crystallization pressures are related to shock pressure and shock stage from S3 to S6. In addition, we set out to determine how melt-vein thickness, which determines the thermal quench rate during shock, affects melt-vein mineralogy. The crystallization pressure constraints, inferred from melt-vein mineralogy, are discussed in the context of shock histories of the samples.

SAMPLES AND METHODS

Eleven L5–L6 chondrites, ranging from shock stage S3 to S6 (Table 1), were obtained from the Center for Meteorite Studies at Arizona State University for investigation. These are Roy, La Lande, Kunashak, Nakhon Pathon, Ramsdorf, Gifu, Waconda, Pinto Mountains, Beaver, Umbarger, and Tenham.

Doubly polished demountable thin sections were prepared and examined optically. Shock effects in olivine and plagioclase were characterized by optical microscopy to determine the shock stage, based on the shock classification system of Stöffler et al. (1991). Of our eleven samples, eight were previously studied and shock-classified by Stöffler et al. (1991). Our shock stages disagree with those of Stöffler et al. (1991) for two samples (Table 1). The chondrite Roy was classified as S3 by Stöffler et al. (1991), whereas the presence of well-developed maskelynite around melt veins leads us to an S5 shock stage. In Umbarger, which was previously classified as S4, we observed blue ringwoodite in melt veins, which implies a shock stage of S6.

The samples were investigated by a combination of

optical petrography using transmitted and reflected light, scanning electron microscopy (SEM) with thermal and field-emission electron sources, electron microprobe analysis (EMPA), and analytical transmission electron microscopy (ATEM). The textures of the melt veins and semi-quantitative analysis of mineral assemblages in the melt veins were determined using a JEOL JSM-840 SEM and a Hitachi S-4700 FESEM, both equipped with an energy dispersive spectroscopy (EDS) system.

Transmission electron microscopy is the primary tool for determining the crystallization assemblages in shock-induced melt veins because most of the crystals are extremely fine grained (sub-μm to several μm). Selected areas containing shock-induced melt veins were cored from thin sections and fixed to copper washer-type supports (3 mm in diameter) and ion-beam thinned until perforation. Ion-thinned samples were coated with 5–10 nm of amorphous carbon to prevent charging of the sample during TEM analysis. Diffraction contrast imaging was employed to characterize the microtexture of the veins and the microstructures of the vein minerals. Mineral phases were identified on the basis of selected area electron diffraction (SAED) and quantitative energy dispersive X-ray spectroscopy (EDS) microanalyses. Details of our procedures for EDS microanalyses were described in previous papers (Xie and Sharp 2004; Xie et al. 2006).

There are two distinct types of veins in the eleven samples: 1) shock-induced melt veins and pockets that contain silicates, and 2) veins that are filled with predominantly iron oxides. The iron oxide veins cross-cut melt veins and represent weathering, probably of metal-sulfide veins that postdated pre-existing silicate melt veins. Shock-induced melt features include veins and pockets. Some melt pockets are interconnected to melt veins, whereas others appear to be isolated. However, we view these features in a planar section and do not know whether they are connected to features out of plane. For simplicity, we will refer to the melt pocket features as melt veins. Shock-induced melt veins and melt pockets that contain silicate minerals or glasses were found in eight of the eleven samples. The remaining three samples (Waconda [S4], Pinto Mountains [S5], and Beaver [S5]) contain veins that are black or dark red in transmitted light, but are metallic gray in reflected light. SEM imaging and EDS show that these veins are composed of Fe-oxide with minor SiO_2. TEM studies were carried out on seven samples, which include Roy (S3–S5), La Lande (S4), Kunashak (S4), Nakhon Pathon (S4), Ramsdorf (S4), Umbarger (S5–S6), and Tenham (S6). For Tenham, we prepared 4 TEM samples, which contain veins ranging in width from 5 μm to 580 μm.

In addition to sample characterization, we used numerical methods to model possible cooling and shock-pressure histories of the samples. The Autodyn 2-D wave propagation code was used to calculate the detailed initial rise of a pressure pulse near a centimeter-wide open fracture in an impact between a planar projectile and target. To provide sufficient resolution, we used a SPH (smooth particle hydrodynamics) cell size of 1 mm, for a total of ~1,000,000 cells. We also used a finite element heat transfer (FEHT) code (Xie et al. 2006) to calculate cooling rates of molten veins as a function of vein width.

Table 1. Petrographic shock classification of 11 chondrites, and shock stage pressure versus melt-vein crystallization pressure.

Eleven L5–L6 chondrites	Shock stage (Stöffler et al. 1991) (GPa)	Crystallization pressure (this study) (GPa)
Roy	S3 (5–20) S5 (30–55)	~20
La Lande	S4 (15–35)	<2.5
Kunashak	S4 (15–35)	<2.5
Nakhon Pathon	S4 (15–35)	<15
Ramsdorf	S4 (15–35)	<15
Gifu	S4	
Waconda	S4	
Pinto Mountains	S5	
Beaver	S5	
Umbarger	S5 (30–55) S6 (45–90)	~18
Tenham	S6 (45–90)	~25

RESULTS

Roy (S3–S5)

Roy, which was previously classified as S3 (Stöffler et al. 1991), has abundant isotropic maskelynite adjacent to the shock-induced veins (Fig. 1a). Some of these maskelynites show flow features (Fig. 1a) indicative of normal glass (Stöffler et al. 1991). The presence of maskelynite and normal plagioclase glass is consistent with shock stage S5 or S6 if the maskelynite occurs throughout the sample. Our sample of Roy contains maskelynite only along melt veins, so strict application of the classification (Stöffler et al. 1991) makes Roy S3 away from the melt vein or S5 along the melt vein. The exclusive occurrence of the maskelynite adjacent to the veins suggests that the transformation of plagioclase to maskelynite is enhanced by the transient high-temperature environment along melt veins.

The textures of melt veins in Roy are quite distinct from those of more highly shocked S6 samples. FESEM images show that the melt veins in Roy have variable metal-sulfide contents that suggest multiple veining events in the same location (Figs. 1b and 1c). These veins contain silicate host-rock fragments, from 1 to 12 μm, in a matrix of metal-sulfide melt (Fig. 1b). The angular to rounded shapes of the silicate fragments suggest that they are cataclastic fragments formed by extensive shear deformation in a pseudotachylite-like vein.

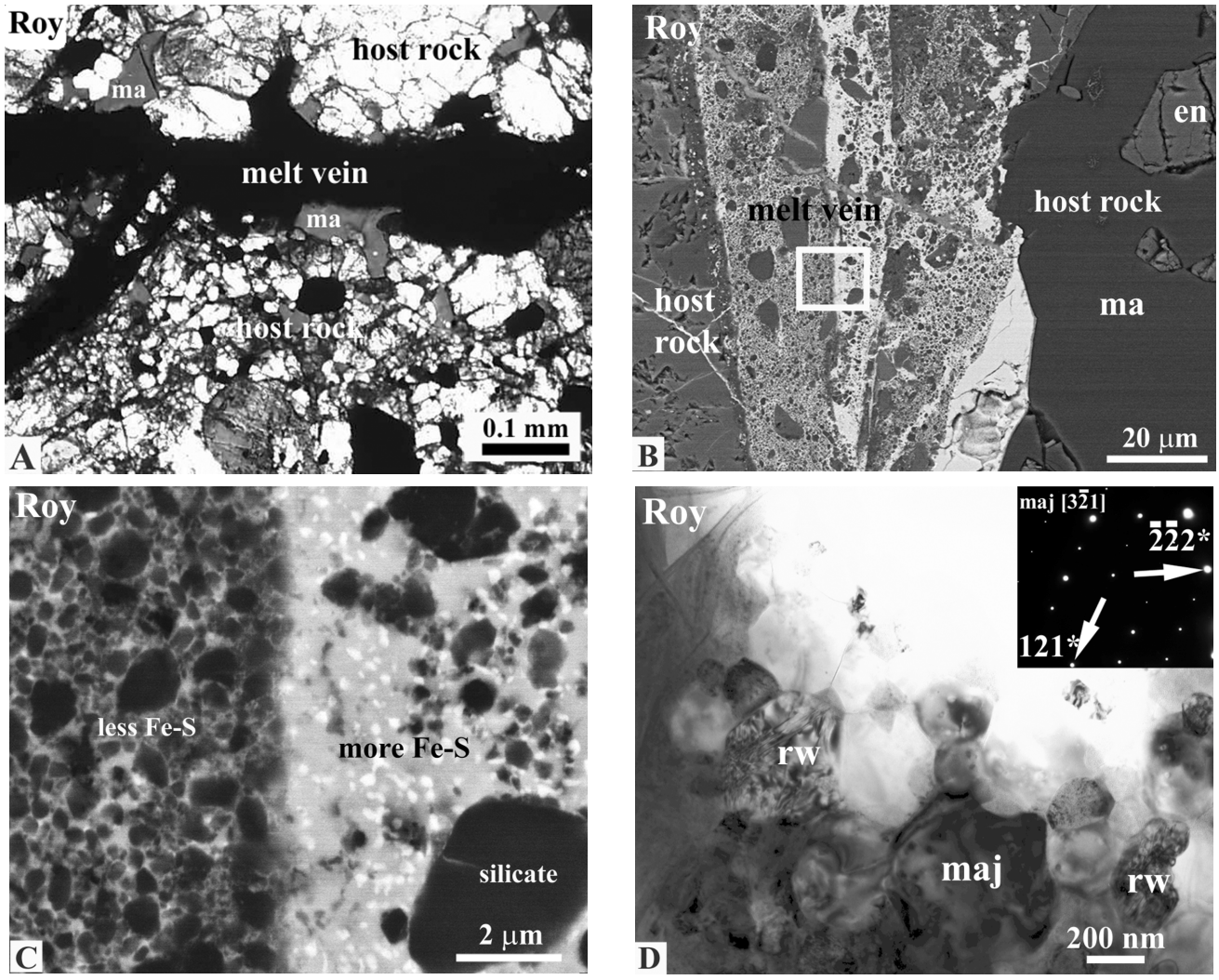

Fig. 1. a) An optical micrograph showing gray isotropic maskelynite (ma) adjacent to the opaque shock-induced melt vein of Roy. b) An FESEM image showing multiple veins in Roy that are distinguished by variations of iron sulfide content. b) An enlarged image of the box in Fig. 1b showing the interface between two veins with different iron sulfide contents. Both veins contain fine silicate grains (dark gray) surrounded by iron sulfide (light gray) and Fe-Ni metal (white). d) A bright-field TEM image showing ringwoodite (rw) and majorite (maj) in a narrow melt vein of Roy at the left edge of the vein complex in Fig. 1b. The inserted diffraction pattern is the [3$\bar{2}$1] zone-axis pattern of the strong diffracting (dark contrast) majorite grain.

The matrices of these veins consist of iron sulfide that was apparently liquid (Figs. 1b and 1c). These textures suggest that most of the veins in Roy were caused by frictional heating to temperatures high enough to melt the metal-sulfide component, but generally not high enough to melt the silicate.

Some veins in Roy were hot enough to create a silicate melt, which subsequently quenched to a high-pressure assemblage. At the left edge of the complex vein in Fig. 1b there is a narrow vein that is dominated by silicate, in which the sulfide liquid formed round droplets. This texture indicates that this narrow vein reached temperatures high enough to form immiscible silicate and metal-sulfide melts. This is confirmed by TEM analysis, which reveals the presence of majorite ($En_{77}Wo_8Fs_{15}$) and ringwoodite (Fa_{27}) (Fig. 1d). The fine-grained intergrowth of these high-pressure minerals is consistent with crystallization from a silicate melt at high pressure. The composition of the majorite is distinctly more calcium rich than the low-Ca pyroxene ($En_{82}Wo_1Fs_{17}$) in the sample, indicating that it did not form by transformation of low-Ca pyroxene, but rather crystallized from a silicate melt at high pressure. Based on the stable liquidus assemblage of majorite plus ringwoodite at ~18–22 GPa (Fig. 9) in the Allende phase diagram (Agee et al. 1995), we infer that this silicate-melt in Roy quenched and crystallized at approximately 18–22 GPa.

Kunashak (S4) and La Lande (S4)

Both Kunashak and La Lande are L6 chondrites consisting of an assemblage of olivine, pyroxene, and

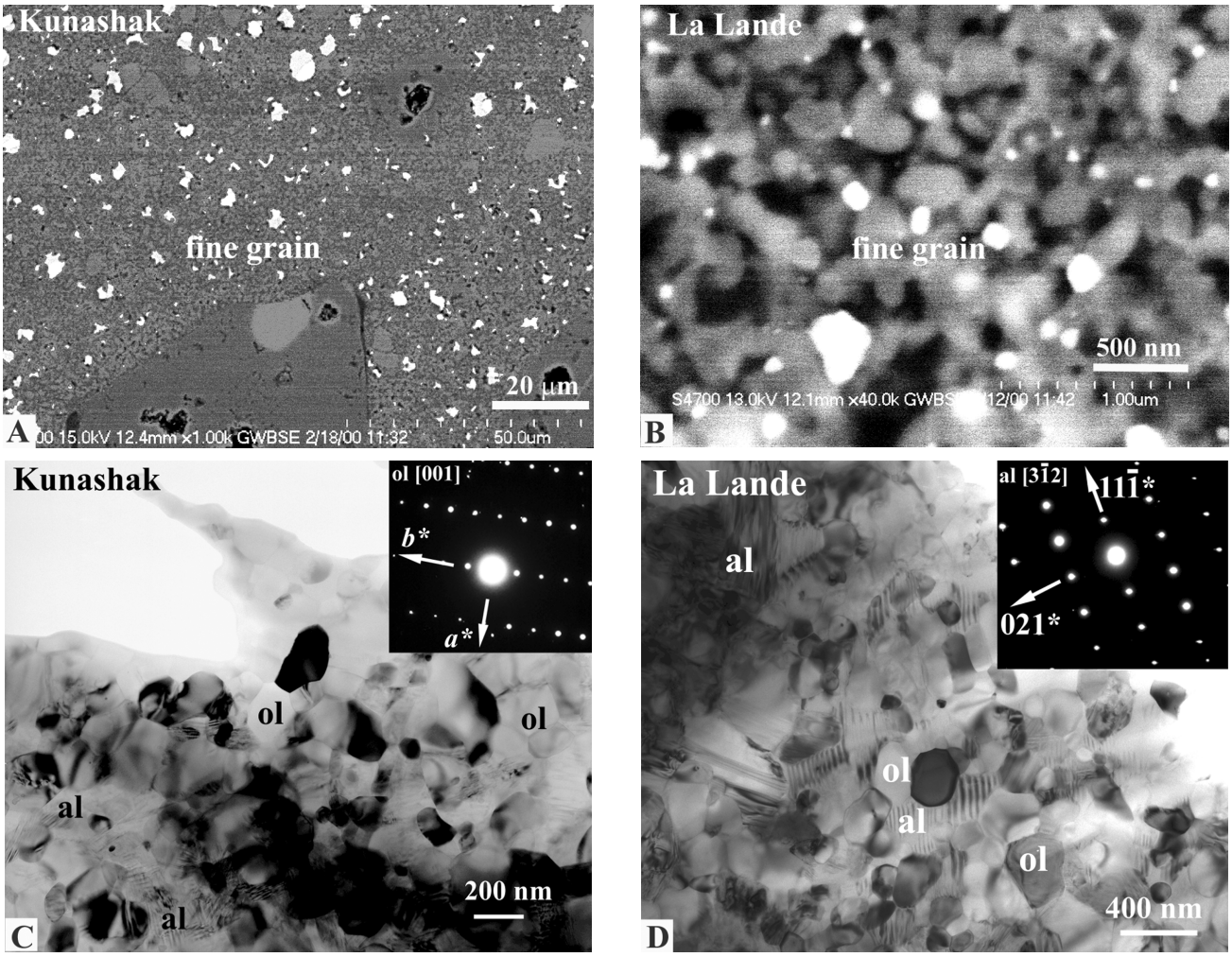

Fig. 2. a) An FESEM image showing fine crystalline silicate in a shock-induced melt vein of Kunashak. The irregular white blebs are metal-sulfide. b) An FESEM image showing fine silicate crystals in the melt vein of La Lande with metal-sulfide blebs (white), olivine (gray) and albite (black). c) A bright-field TEM image showing olivine (ol) intergrown with albite (al) in the melt vein of Kunashak. The inserted SAED pattern shows the [001] zone axis of the dark-contrast olivine grain in center of the image. f) A bright-field TEM image of olivine (ol) intergrown with albite (al) in the melt vein of La Lande. The diffraction pattern shows the [3$\bar{1}$2] zone axis of albite grain in upper left of image. Many of the albite grains have fringe contrasts that indicate planar defects.

plagioclase, with minor amounts of metal and troilite. Both olivine and pyroxene have abundant shock-induced irregular and planar fractures, and show typical mosaicism as indicated by a pronounced irregular optical extinction. Both chondrites contain black shock-induced melt veins or melt pockets, which have rounded blebs of metal-sulfide. Few plagioclase grains in Kunashak are optically isotropic, indicating that very little maskelynite is present. Because most plagioclase grains show sharp extinction, we assigned a shock stage S4 to Kunashak. Plagioclase grains in La Lande also show sharp extinction in crossed polarized light, indicating a lack of maskelynite. As that previously assigned by Stöffler et al. (1991), we assigned a shock stage S4 to La Lande.

Kunashak and La Lande are grouped together because they have similar melt vein textures and melt crystallization assemblages. The silicates in the melt vein are so fine-grained that the spatial resolution of a conventional SEM was not sufficient to resolve the grains and distinguish this material from glass. Field emission SEM is able to show that the melt veins in both chondrites contain fine silicate crystals, subrounded fragments of the host rock, and irregular metal-sulfide blebs (Figs. 2a and 2b). The melt veins in Kunashak and La Lande are not dominated by metal-sulfide, as in Roy, but rather the metal-sulfide occurs as irregular blebs, suggesting droplets of metal-sulfide liquid in a matrix of partially molten silicate. This texture suggests that the melt-vein temperatures were high enough for complete melting of metal-sulfide and partial melting of the silicate.

The extremely fine-grained silicates in the melt veins of Kunashak and La Lande were identified with TEM by using electron diffraction and quantitative EDS. These fine silicates consist of olivine and albite both in Kunashak (Fa_{22} and

$Ab_{95}An_2Or_3$) (Fig. 2c) and La Lande (Fa_{22} and $Ab_{96}An_2Or_2$) (Fig. 2d). The olivines are randomly oriented subhedral crystals that are ~200 nm in size and defect-free (Figs. 2c and 2d). The albite, which was indexed using the C-1 structure of triclinic albite, commonly shows evidence of planar defects (Figs. 2c and 2d) that have not been characterized in detail, but may be albite twins. The melt veins of both chondrites also contain Ca-poor and Ca-rich pyroxenes, which are unmelted fragments of host rock. In Kunashak these pyroxenes are ($En_{78}Wo_2Fs_{20}$) and ($En_{62}Wo_{23}Fs_{15}$), whereas in La Lande the pyroxenes are ($En_{77}Wo_1Fs_{22}$) and ($En_{56}Wo_{33}Fs_{11}$).

Although olivine is the liquidus phase up to ~15 GPa in the Allende phase diagram (Fig. 9), the presence of albite indicates low-pressure crystallization. The upper pressure stability limit of albite is about 2.5 GPa at ~900 °C, defined by the reaction of albite to form jadeite plus quartz (Thompson and Tracy 1979). The olivine plus albite assemblage thus indicates melt-vein crystallization at pressures less than about 2.5 GPa. These assemblages probably crystallized after pressure release and therefore do not constrain the peak shock pressures of La Lande or Kunashak.

Nakhon Pathon (S4) and Ramsdorf (S4)

We assigned shock stage S4 to Nakhon Pathon based on the lack of maskelynite, abundant shock-induced irregular and planar fractures in olivine and pyroxene crystals, and strong mosaicism in these crystals. Only a few tiny plagioclase crystals in Nakhon Pathon are isotropic under crossed polarized light, whereas most plagioclase is anisotropic and therefore crystalline.

Ramsdorf has been previously studied and assigned different shock stages. Recrystallized olivine and pyroxene and abundant silicate glass led Begemann and Wlotzka to conclude that Ramsdorf was altered by shock-induced thermal metamorphism. Stöffler et al (1991) classified Ramsdorf as S4, whereas Yamaguchi et al. (1996) interpreted Ramsdorf as having experienced two shock events of different shock grades. The first event with a shock stage greater than S6 (~75–90 GPa) produced most of the impact melts. The second event with a shock stage of S3–S4 (15–35 GPa) formed minor interconnected glassy veins. In our Ramsdorf sample, olivine and pyroxene grains show undulatory extinction and strong mosaicism. Only a few large plagioclase crystals were completely transformed to maskelynite, whereas most are anisotropic. Therefore, we agree with the S4 shock stage assigned by Stöffler et al. (1991). The local melting of the chondrite may simply reflect local thermal heterogeneities, rather than pressure heterogeneities, as suggested by Yamaguchi et al. (1996). This will be discussed in detail later in the paper.

Low-resolution SEM images show that melt veins in both Nakhon Pathon and Ramsdorf contain melt matrix, host rock fragments, and metal-sulfide blebs (Figs. 3a and 3b). In Nakhon Pathon, the metal-sulfide blebs are predominantly round, indicating the presence of immiscible silicate and sulfide melts (Fig. 3a). However, in Ramsdorf the metal-sulfide blebs range from irregular to round, indicating that the silicate was partially to mostly molten within the melt veins (Fig. 3b).

TEM data shows abundant silicate glass in the melt vein of Nakhon Pathon. Spheroidal metal-sulfide droplets (Fig. 3c) and tear-shaped grains (Fig. 3d) occur in the silicate glass, indicating rapid quench. EDS data show that the tear-shaped grains contain Fe, S, Si, and O (Fig. 3d). TEM electron diffraction and quantitative EDS also confirmed that the melt veins of both chondrites contain olivine and clinopyroxene, which crystallized from the silicate melts. In Nakhon Pathon (Fig. 3e) the olivines are (Fa_{25}) and the clinopyroxenes are ($En_{80}Wo_5F_{15}$), whereas in Ramsdorf (Fig. 3f) the olivines are (Fa_{21}) and the clinopyroxenes are ($En_{78}Wo_4F_{19}$). The clinopyroxenes in Ramsdorf are euhedral, ~300 nm in size, and embedded in silicate glass. The diffraction patterns from these low-Ca clinopyroxenes have $h + k \neq 2n$ reflections such as *10-1* and *010* (Fig. 3e) and *120* (Fig. 3f), which are only allowed in the primitive $P2_1/c$ unit cell. Clinopyroxene plus olivine is a subsolidus assemblage at pressure up to 15 GPa (Fig. 9). Although this assemblage is generally associated with low-pressure crystallization, the melt veins in both Nakhon Pathon and Ramsdorf L chondrites could have crystallized at pressure up to 15 GPa, which is reasonable for an S4 sample.

Umbarger (S5–S6)

Our results for Umbarger have been published previously (Xie and Sharp 2004; Xie et al. 2002) and are only briefly summarized here. Although Stöffler et al. (1991) assigned Umbarger a shock stage of S4, we observed strong mosaicism in olivine and abundant maskelynite, indicating a shock stage of S5. In and adjacent to melt veins, glassy plagioclase with flow textures and polycrystalline ringwoodite suggest a shock stage S6. Vein networks are pervasive throughout our thin section, but most of these are Fe-oxide-rich alteration veins.

The melt veins that are present have a matrix that consists of fine-grained silicates (Fig. 4). Electron diffraction and EDS confirm that this assemblage contains akimotoite, ringwoodite, and Ca-rich clinopyroxene (Xie and Sharp 2004). The clinopyroxenes in these veins are single crystals that occur interstitially between akimotoite and ringwoodite crystals. This texture indicates that the pyroxene was the last mineral to crystallize from the melt. If these pyroxenes had formed from the transformation of some higher-pressure precursor such as silicate perovskite, nucleation along grain boundaries would be expected to produce polycrystalline pyroxene pseudomorphs after the higher-pressure phase.

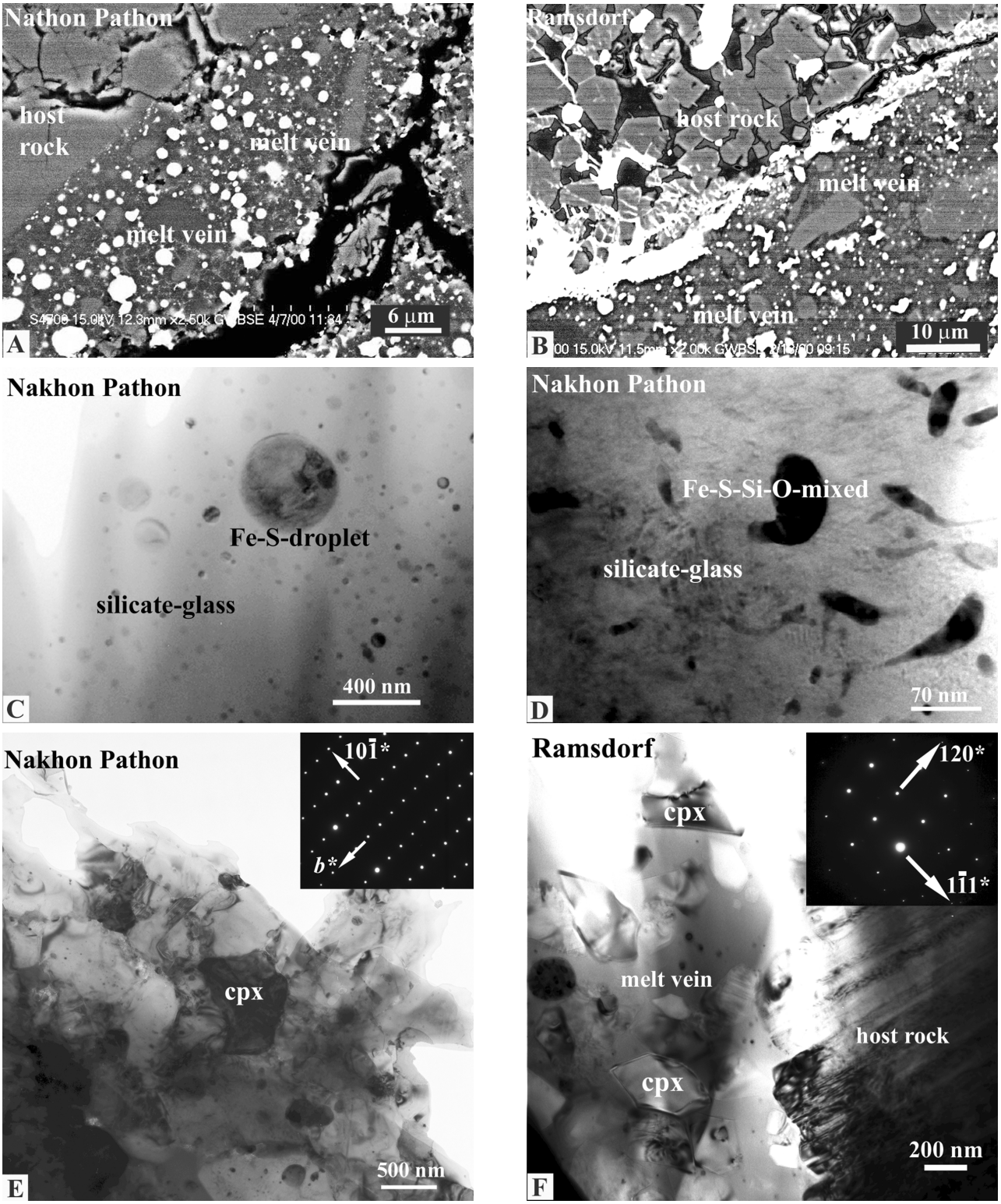

Fig. 3. a) An FESEM image showing a melt vein in Nakhon Pathon containing host silicate fragments in a silicate matrix mixed with round metal-sulfide droplets (white). b) An FESEM image of a melt vein in Ramsdorf containing a silicate matrix mixed with irregularly shaped metal-sulfide blebs and host rock fragments. c) A bright-field TEM image of spherical metal-sulfide droplets in silicate glass from the edge of the melt vein in Nakhon Pathon. d) A bright-field TEM image showing tear-shaped grains of mixed Fe, S, Si, and O in an glass matrix in the melt vein of Nakhon Pathon. e) A bright-field TEM image of clinoenstatite (cpx) in the melt vein of Nakhon Pathon. The SAED pattern shows the [101] zone axis of the strongly diffracting clinoenstatite in the center. f) A bright-field TEM image of euhedral clinoenstatite (cpx) in silicate glass of Ramsdorf. The SAED pattern is the [2$\bar{1}\bar{3}$] zone-axis pattern of clinoenstatite (cpx).

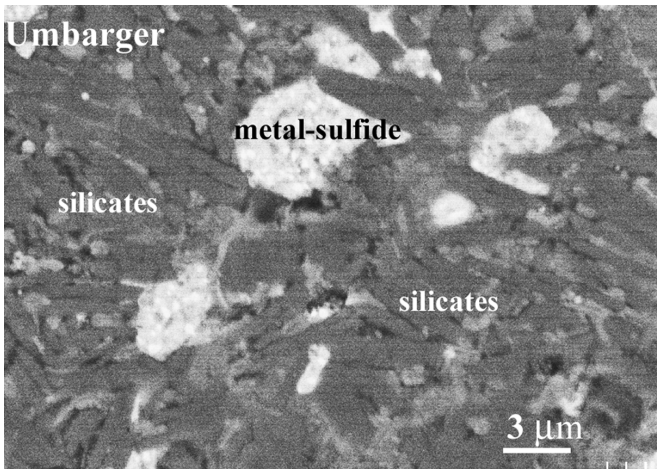

Fig. 4. An FESEM image of the melt-vein matrix in Umbarger shows elongated akimotoite crystals (dark gray) intergrown with ringwoodite (light gray) and droplets of metal-sulfide.

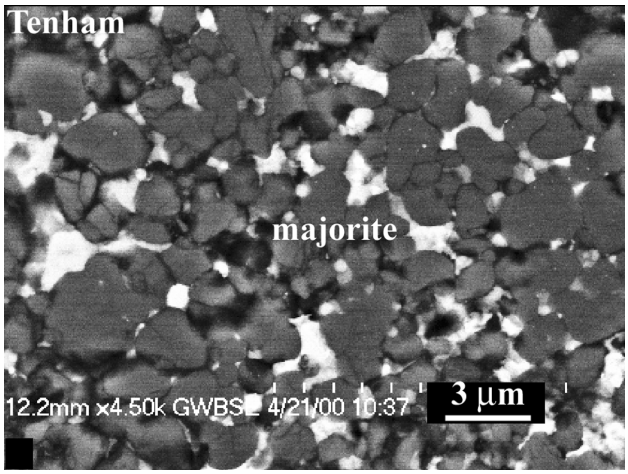

Fig. 5. An FESEM image of the vein interior region in Tenham showing equant majorite crystals and irregular oxide grains and metal-sulfide blebs (white).

Unlike most highly shocked chondrites, Umbarger has large variations in shock-melt composition, with local FeO-SiO_2-rich zones that crystallized Fe_2SiO_4-spinel and stishovite at high pressure (Xie et al. 2002).

The crystallization pressure for the silicate melt in Umbarger melt veins is difficult to interpret because the crystallization assemblage contains subsolidus phases. Akimotoite does not appear at all in the Allende phase diagram (Agee et al. 1995). Akimotoite is a subsolidus phase that occurs together with ringwoodite between 18 and 25 GPa in the $MgSiO_3$-Mg_2SiO_4 system (Gasparik 1992). Similarly, Ca-rich clinopyroxene is metastable relative to majorite garnet near the liquidus at high pressure, but is stable as a subsolidus phase up to about 18 GPa (Oguri et al. 1997). The assemblage in Umbarger is likely a result of metastable crystallization at high pressure during rapid quench. The crystallization pressure was probably close to 18 GPa, which is the upper stability limit of pyroxene and the lower stability limit of akimotoite plus ringwoodite. The Fe_2SiO_4-spinel + stishovite assemblage in the FeO-SiO_2-rich melts of Umbarger is consistent with crystallization of the melt-vein matrix at the pressure approximately 18 GPa (Xie and Sharp 2004).

Tenham (S6)

Many of our results for Tenham have been published previously (Xie et al. 2006) and are summarized here along with new results based on the characterization of melt veins of various sizes. Our thin section of Tenham contains a dense network of melt pockets and black veins from 5 μm to 1.5 mm thick. Most of the pockets and thicker veins enclose small rounded multiphase fragments of host rock that contain blue ringwoodite grains. Plagioclase throughout the sample has been transformed to maskelynite or normal glass. Abundant ringwoodite in the melt veins and maskelynite throughout the sample indicate a shock stage of S6. We have used TEM to investigate the mineral assemblages that crystallized from veins ranging in width from 5 to 580 μm.

Large melt veins in Tenham contain two high-pressure mineral assemblages. The vein edge (~30 μm wide) consists of a mixture of equant and irregularly shaped grains with a few rounded metal-sulfide droplets, while the center of the melt vein (550 μm wide) consists of equant silicate crystals and irregularly shaped metal-sulfide blebs (Fig. 5). TEM imaging and electron diffraction reveal that the vein interior consists of predominantly majorite plus magnesiowüstite (Xie et al. 2006), which is consistent with previous studies (Price et al. 1979; Putnis and Price 1979; Langenhorst et al. 1995; Tomioka and Fujino 1997). The vein-edge consists of vitrified silicate-perovskite, ringwoodite, akimotoite, and majorite (Xie et al. 2006). The pressure stabilities of both assemblages are similar: the melt-vein edge crystallized at approximately 23–25 GPa, whereas the vein interior crystallized at about 21–25 GPa. These assemblages suggest that the melt vein either crystallized at an equilibrium shock pressure of approximately 25 GPa or during a relatively slow pressure release (Xie et al. 2006).

In order to further investigate the early stages of melt-vein crystallization, we investigated a set of much thinner veins that would have quenched much faster than the 580 μm vein described above. The mineral assemblages in these narrow veins are quite different and indicate that melt-vein mineralogy can vary with vein width in a given sample. In one TEM sample, a single vein that varies in width from 5 μm to 30 μm (Fig. 6a) contains predominantly silicate glass and metal-sulfide droplets in the 5 μm region (Figs. 6a and 6b), ~200 nm olivine crystals and metal-sulfide grains in the 10 μm wide region (Figs. 6a, 6c, and 6d) and ringwoodite, glass, and olivine in the 30 μm region (Figs. 6a, 6e, and 6f). In

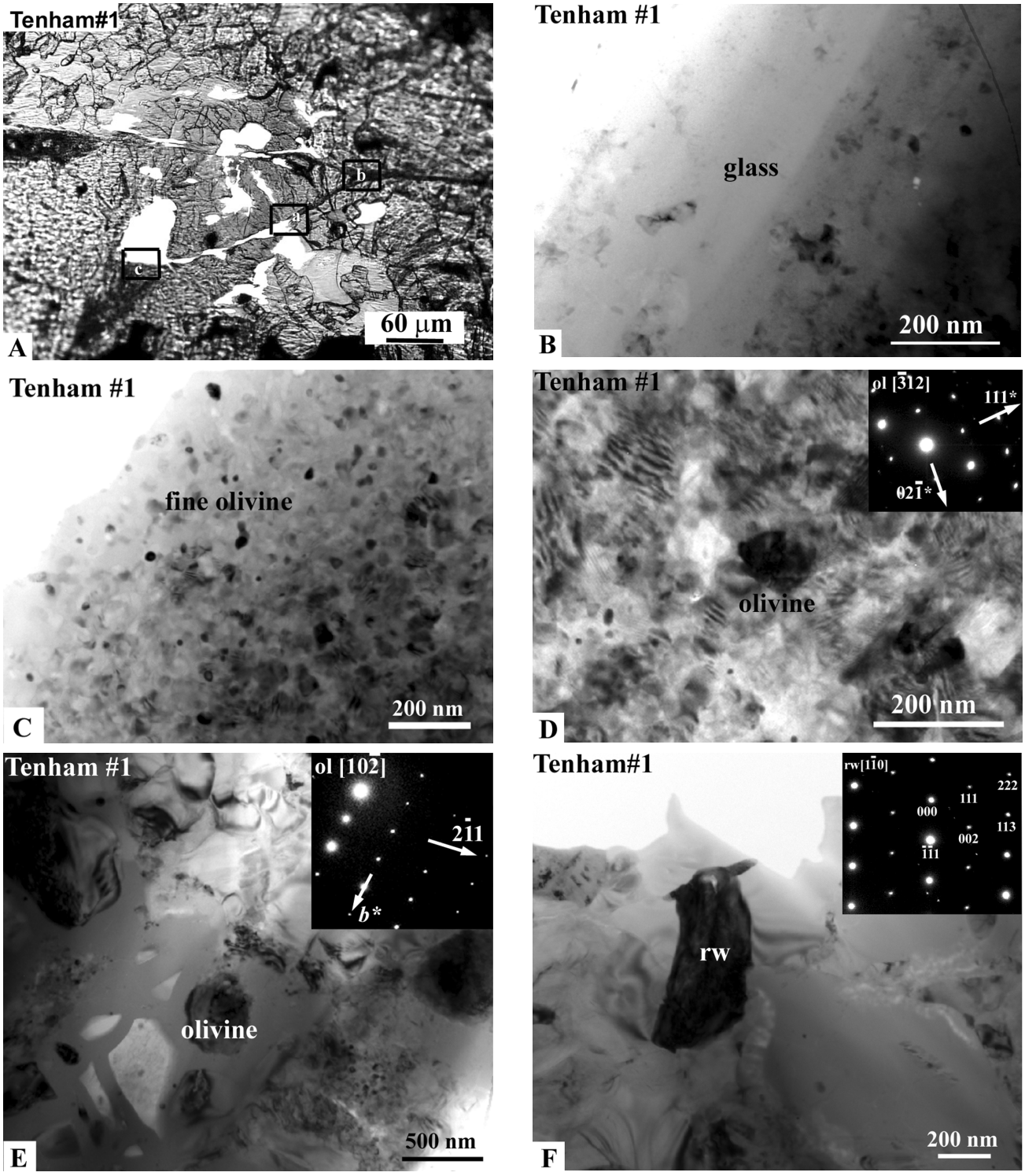

Fig. 6. a) An optical micrograph of Tenham TEM sample #1 showing a branching melt vein of variable width. The widths of vein segments in the boxes a, b, c are ~5 μm, 10 μm, and 30 μm, respectively. b) A bright-field (BF) TEM image showing silicate glass and unidentified grains in the 5 μm wide vein (box a in 6a). c) A BF TEM image of fine olivine grains in the 10 μm wide vein (box b in 6a). d) A higher-magnification BF TEM image of fine olivine grains in the 10 μm wide vein segments (box b in 6a). The inserted diffraction pattern shows the [3̄12] zone axis of the dark olivine in center of the image. e) A BF TEM image showing olivine crystals and other unidentified grains in silicate glass in 30 μm wide vein (box c in 6a). The inserted SAED pattern shows the [10$\bar{2}$] zone axis of olivine. f) A BF TEM image showing ringwoodite (rw) and other unidentified phases in silicate glass in 30 μm wide vein. The inserted SAED pattern shows the [1$\bar{1}$0] zone axis of ringwoodite.

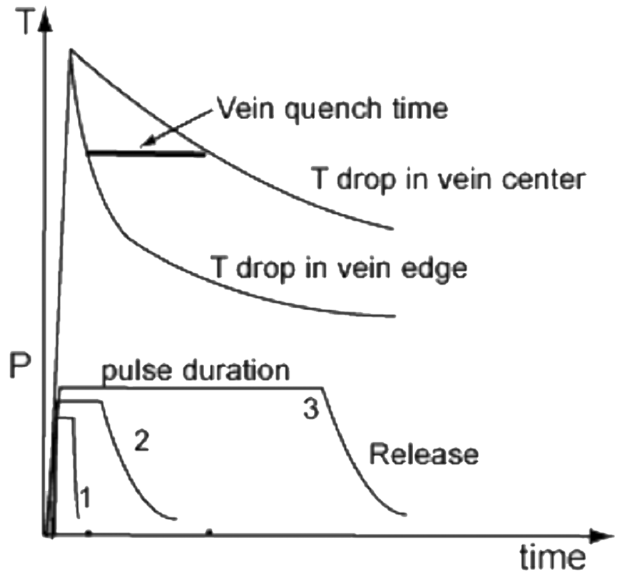

Fig. 7. Pressure and temperature versus time profiles for three quench scenarios: 1) the pressure pulse is much shorter than the total quench time such that most of the quench occurs after pressure release, 2) the pressure pulse is shorter than the total quench time resulting in quench through the equilibrium shock pressure and into pressure release, 3) the pressure pulse duration exceeds the total quench time and crystallization occurs at equilibrium shock pressure.

another Tenham TEM sample, an 8 μm wide vein is connected to a 30 μm wide region and contains similar mineralogical variations. The 8 μm wide vein region contains ~200 nm olivine crystals and metal-sulfide grains, while the 30 μm wide vein region contains ringwoodite, olivine, and other phases.

The highly variable assemblages in these thin melt veins suggest that the pressure was changing significantly during the relatively short period of melt-vein quench. The glassy material in the 5 μm wide vein suggests a quench rate that was too rapid for silicate crystals to form. The 8 to 10 μm vein regions, which contain olivine, indicate crystallization at a pressure less than about 15 GPa. The 30 μm wide vein-regions, which contain ringwoodite and olivine, suggest variable crystallization pressures from less than 15 GPa up to 20 GPa. These pressure variations, which occurred over a narrow time interval during the shock, suggest pressure variations much greater than those implied by the crystallization assemblages in the 580 μm wide vein.

DISCUSSION

Shock-induced melt veins result from the localized mixing and melting of coexisting minerals, and the subsequent quench of immiscible silicate and metal-sulfide melts. Understanding when a melt vein forms and crystallizes relative to shock loading and pressure release is necessary to relate crystallization pressures to shock pressure. We will discuss melt-vein crystallization, crystallization pressure constraints, the relationship between crystallization pressure and shock pressure, and the anomalous assemblages found in the very thin veins of Tenham.

Melt-Vein Formation and Quench

There are several possible mechanisms for melt vein formation. Shock-wave interactions between different shock impedance materials may cause localized melting, which is most pronounced at the interface of metal-troilite and silicates, and the interface of minerals and pore space (Kieffer 1971; Stöffler et al. 1991; Schmitt 2000; Sharp and De Carli 2006). Friction by shear along the contacts of materials of vastly contrasting shock impedance and along fractures may also produce local melting (Gault et al. 1968; Kieffer 1975; Grady et al. 1975; Spray 1998; Kenkmann et al. 2000). Adiabatic shear can produce temperatures that are thousands of degrees hotter in shear regions than in immediately adjacent material (Grady et al. 1975). Although adiabatic shear is often associated with the release phase of a pressure pulse (Nesterenko 2001), we will present calculations that show that relatively low pressures may also occur during the complex rise of a pressure pulse in a fractured rock.

The response of a heterogeneous material to shock compression is extremely complex when viewed on a nanosecond time scale and on a micrometer distance scale. The shock front is chaotic, with order-of-magnitude differences in initial pressure due to shock wave interactions among grains of different shock impedance and with small cracks and pores. However, these initial pressure differences quickly dampen out to an equilibrium peak pressure. The term "peak pressure," as used by most shock-wave specialists, refers to the continuum pressure or equilibrium pressure. If two Tenham-like bodies collide at a relative velocity of 2.1 km/s, the continuum pressure at the point of impact will be ~25 GPa. Assuming a millimeter grain size (including cracks and pores), the initial chaotic distribution of pressures, spanning the range from ~15 GPa to >100 GPa, will equilibrate to ~25 GPa within <1 μs. Therefore, the initial pressure fluctuations on the scale of the grain size are generally neglected (Fig. 7). For a large impact, the pressure near the impact is effectively constant and corresponds to the equilibrium shock pressure in the simple flatted-top pressure model (Fig. 7).

However, there is an additional complication. Most rocks, and probably meteorite parent rocks, are fractured. Pre-existing fractures can locally perturb the shock pressure history producing a transient pressure decay as material flows into the open fracture. In order to quantitatively assess the effects of open fractures, we have used the Autodyn computer code to calculate the pressure history in the vicinity of a fracture ~1 cm wide in an impact between a planar projectile and target (Fig. 8). The presence of the fracture caused a

decay of the initial impact pressure over about 10 μs to ~6 GPa, as the pressure was relieved by flow into the void. The pressure then rose over ~50 μs to the continuum pressure of 12 GPa (Fig. 8). Shock propagation in a real fractured rock will be much more complex than our calculation, which was based on a simple single-fracture model. A more realistic calculation of the effects of multiple fractures would require a supercomputer. However, our model calculation supports analytic estimates that multiple open fractures (meter scale fracture spacing and maximum fracture opening of ~1 cm) would result in complex stress oscillations over a period of 0.1 to 1 ms during the rise of stress to the continuum (equilibrium) level. It seems reasonable to suggest that melt-vein formation may occur during this chaotic pressure equilibration phase, particularly for the thin veins with short quench time (less than 10 μs).

The word "equilibrium," as in equilibrium (continuum) pressure, should be used with caution; thermodynamic equilibrium is not implied, and the chaotic distribution of initial temperatures equilibrates much more slowly than the chaotic pressure. The temperature difference between the melt vein and host rock determines the rate at which the melt vein quenches (Langenhorst and Poirier 2000; Xie et al. 2006). Quenching begins as soon as the vein forms, independent of the pressure pulse duration. The temperature decrease caused by adiabatic decompression is small compared to that caused by thermal conduction (Langenhorst and Poirier 2000; De Carli et al. 2002; Xie et al. 2006) and therefore the quench is not driven by or necessarily coincident with pressure release. The solidification of the melt vein starts from the vein edge and ends in the vein center (Fig. 7). The time required to quench an entire melt vein can be estimated with thermal modeling (Langenhorst and Poirier 2000; Xie et al. 2006).

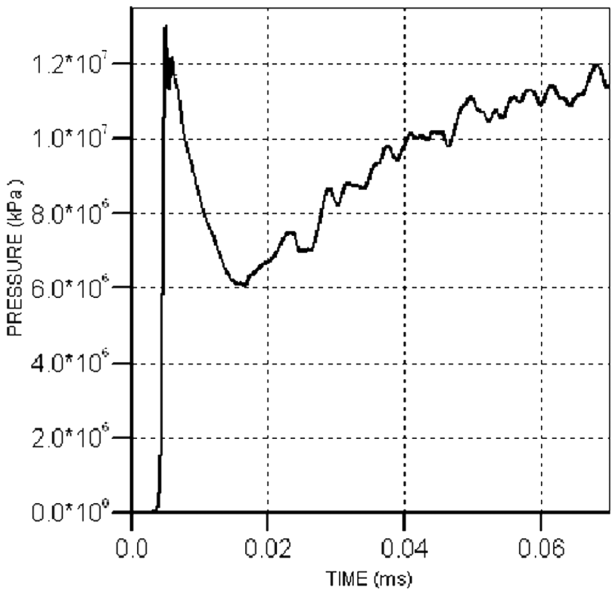

Fig. 8. Pressure history calculated by the Autodyn computer code near a centimeter-wide open fracture showing initial pressure of ~12 GPa decaying to ~6 GPa over 10 μs and then rising to the continuum pressure of ~12 GPa over 50 μs.

Crystallization Pressure

Although solid-state high pressure phase transitions in silicates are very sluggish at modest temperatures, the crystallization of an ultramafic silicate melt in a shock vein is likely to occur closer to equilibrium conditions because of rapid nucleation in a supercooled liquid and rapid diffusion in ultramafic melts at very high temperatures. As previously noted, phase diagrams obtained from static high-pressure experiments can be used to constrain the conditions of melt-vein crystallization (Chen et al. 1996). The approach is not to assume chemical equilibrium and look for equilibrium assemblages, but rather to constrain the crystallization pressure from the overall pressure stabilities of the minerals that crystallized from the melt. Subliquidus and subsolidus phases such as akimotoite, olivine, and clinopyroxene in the melt veins are interpreted as resulting from metastable crystallization from supercooled liquids during rapid quench in shock veins (Langenhorst and Poirier 2000; Xie and Sharp 2004; Xie et al. 2006). However, the pressure stabilities of these metastable phases still provide constraints on crystallization pressure.

There are limited high-pressure experimental data appropriate for interpreting L-chondrite compositions. These include data for the Allende CV carbonaceous chondrite (Agee et al. 1995; Asahara et al. 2004), the Kilburn-Hole peridotite KLB-1 (Zhang and Hertzburg 1994), and the Mable L chondrite (Chen et al. 2004b). For simplification, we select the Allende phase diagram (Agee et al. 1995) for interpretation of our data.

The range of silicate crystallization assemblages seen in our samples can be grouped into three crystallization-pressure regimes on the Allende phase diagram (Fig. 9). The first group includes Tenham (S6), Roy (S3–S5), and Umbarger (S5–S6), where the veins contain well-known high-pressure minerals, such as ringwoodite, majorite, akimotoite, etc., indicating crystallization under high-pressure and high-temperature conditions. This group has the highest crystallization pressure range from about 18 to 25 GPa, with an unknown error of probably a few GPa. The second group includes Ramsdorf (S4) and Nakhon Pathon (S4) whose veins contain olivine and clinopyroxene, which are not generally considered high-pressure phases but are stable to pressures up to 15 GPa (Fig. 9). Because the veins in Ramsdorf and Nakhon Pathon are shock features, it should not be automatically concluded that crystallization of olivine and pyroxene occurred at ambient pressure. The lack of plagioclase suggests that crystallization probably occurred at elevated pressure, but the lack of common high-pressure

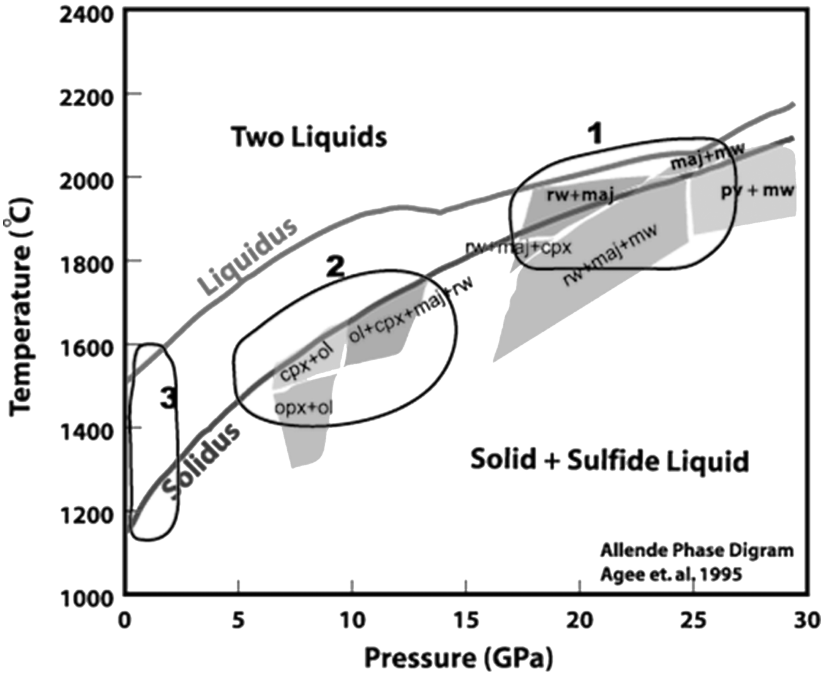

Fig. 9. Three crystallization pressure regions of the shock-induced melt veins are illustrated on a simplified version of the Allende phase diagram (Agee et al. 1995). 1) Crystallization region for Tenham (S6), Roy (S3–S5), and Umbarger (S5–S6). 2) Crystallization region for Ramsdorf (S4) and Nakhon Pathon (S4). 3) Crystallization region for Kunashak (S4) and La Lande (S4). Ol = olivine, cpx = clinoenstatite, rw = ringwoodite, maj = majorite, mw = magnesiowüstite, pv = perovskite.

minerals such as wadsleyite or majorite indicate that the pressure was significantly lower than that of the first group. Therefore the crystallization pressures for melt veins in Ramsdorf and Nakhon Pathon are not well constrained, but were likely between 2.5 and 15 GPa. The third group includes Kunashak (S4) and La Lande (S4), where veins contain olivine and albite. The assemblage of olivine plus albite corresponds to crystallization pressure less than about 2.5 GPa, the upper pressure stability limit of albite (Thompson and Tracy 1979).

The crystallization assemblages in a given melt vein will depend on the time required for melt vein quench versus the duration of high shock pressures. If one assumes a simple shock model with a flat-topped pressure pulse, one can think of crystallization in terms of three scenarios (Fig. 7): 1) If the shock pressure pulse duration is longer than quench time, the melt vein will crystallize at the constant equilibrium-shock pressure. 2) If the pressure pulse duration is similar to or somewhat shorter than quench time, melt-vein crystallization will begin at the equilibrium-shock pressure and continue into pressure release. 3) If the shock pressure pulse is much shorter than the quench time, melt-vein crystallization will occur during and after pressure release. These scenarios should be reflected in the melt-vein mineralogy across the melt veins and pockets. If crystallization occurs at constant pressure, we should see the same assemblage throughout a given melt vein or assemblages that reflect constant pressures. If crystallization occurs during pressure release, we should see an assemblage change from the vein edge to vein center that reflects a decrease in crystallization pressure, with a lower pressure assemblage in the vein center. Therefore, if we see evidence for a narrow crystallization-pressure range throughout the large melt vein, we can conclude that the crystallization pressure probably represents the equilibrium-shock pressure. If we see the same low-pressure assemblage throughout the vein, we can conclude that crystallization occurred after pressure release. If we see a lower-pressure assemblage in vein center relative to the vein edge, we can conclude that crystallization occurred during pressure release.

Mineral assemblages of the melt veins studied here show some variations in assemblage, but no clear evidence that crystallization occurred over a large pressure decrease. In the example of the thick vein in Tenham, which has an assemblage change from silicate-perovskite plus akimotoite plus ringwoodite to majorite plus magnesiowüstite, the pressures corresponding to these assemblages are both close to ~25 GPa and therefore do not necessitate crystallization during a large pressure release (Xie et al. 2006), but a minor pressure decrease cannot be ruled out. In the case of Umbarger, two distinct mineral assemblages occur because of compositional heterogeneities in the melt, not because of significant differences in crystallization pressure. There is no systematic mineralogical change between the melt-vein edge and center, so we infer that Umbarger also crystallized at its equilibrium shock pressure (Xie and Sharp 2004). Roy has a narrow vein in which silicate melted and then crystallized to

majorite plus ringwoodite. This constant assemblage suggests that this narrow vein in Roy crystallized rapidly and over a narrow pressure range. In the case of Nakhon Pathon and Ramsdorf, the assemblages observed do not constrain the crystallization pressure sufficiently to distinguish between crystallization at the equilibrium shock pressure or during pressure release. Therefore, the melt veins in these samples only constrain the shock pressure to be less than 15 GPa during crystallization. In the case of Kunashak and La Lande, the mineral assemblage of olivine and albite are constant across the vein, indicating that crystallization occurred at a pressure below 2.5 GPa and probably that vein formation occurred after pressure release. Again, the veins provide no upper constraints on the shock pressure.

Crystallization Pressure versus Shock Stage

Samples selected for this study have shock stages S3 to S6, corresponding to shock pressures ranging from 5–10 GPa for the onset of S3 to greater than 45–55 GPa for the onset of S6, according to the calibration of Stöffler et al. (1991). However, this study indicates melt-vein crystallization pressures did not exceed approximately 25 GPa (Table 1) for any of these samples. The melt vein in Roy (S3) crystallized at a pressure of 18–22 GPa, which is at the high end of the calibrated S3 pressure (5–10 to 15–20 GPa) of Stöffler et al. (1991). The crystallization pressures of Nakhon Pathon (S4) and Ramsdorf (S4) may have been as high as ~15 GPa, which is lower than the S4 calibration pressure (15–20 to 30–35 GPa). The melt vein of Umbarger (S5 to S6) crystallized at approximately 18 GPa, which is much lower than the S5–S6 calibration pressure (30–35 to 75–90 GPa). The melt veins of Tenham, the most highly shocked sample, crystallized at an equilibrium shock pressure of approximately 25 GPa, which also much lower than the S6 calibration pressure (45–55 to 75–90 GPa). One might infer that the discrepancy between the crystallization pressures and the shock pressure calibrated for S6 samples could be a result of crystallization during pressure release from pressures in excess of 50 GPa. If this were the case, one would expect to observe an assemblage dominated by silicate perovskite in the rapidly cooled vein edges and low-pressure phases such as olivine and pyroxene in the slowly cooled centers of wide veins. However, there are insufficient mineralogical variations from vein edge to vein center in Tenham and Umbarger to support the hypothesis of crystallization during pressure release.

The discrepancy between the shock pressure inferred from melt-vein crystallization and that from shock-recovery experiments may be due to the limitations of shock-recovery experiments. The durations of laboratory shock experiments are short (a few microseconds) compared to natural impacts (up to several seconds). Shock duration is critical for kinetic processes such as phase transformations, making direct comparison of transformation pressures inappropriate between nature and experiment (Gault et al. 1968; De Carli 1968; Chao 1968; Stöffler 1972; Melosh 1989; De Carli et al. 2002). In addition, the multiple-reflection loading paths used in the shock-recovery experiments differ substantially from the direct loading paths of natural events. For a given shock pressure, the internal energy increase is much higher for the direct loading path than for the reflected shock loading path (Tomeoka et al. 1999; De Carli et al. 2002; Bowden 2002). When one takes into account the longer duration of natural shock events, one may infer that shock effects that involve a phase transition, such as maskelynite formation, will occur at a lower pressure in nature than in laboratory shock experiments.

The abundance of shock deformation and phase transformation features near and within melt veins suggest these metamorphic effects are strongly temperature dependant, rather than only pressure dependent. Abundant maskelynite was found adjacent to the shock-induced veins of Roy, but it is not found elsewhere in the sample (Fig. 1a). Polycrystalline ringwoodite aggregates, interpreted to be the result of a solid-state transformation of olivine entrained in the melt vein, are found only in the melt veins of Umbarger. In Tenham (S6), where a dense network of melt veins runs throughout the sample, polycrystalline ringwoodite aggregates are easily seen in melt veins, and highly deformed maskelynite or normal plagioclase glass is seen throughout in the sample. All these observations indicate that temperature is important for phase transformations. Stöffler et al. (1991) attribute similar variations to local temperature and pressure excursions, but the limited distribution of phase transformations to melt-vein regions may simply reflect thermal heterogeneities at equilibrium shock pressure.

Thin versus Thick Melt Veins

As we have discussed, the crystallization history of any shock vein will depend on vein thickness, which determines the quench time. Shock veins cool predominantly by thermal conduction to the cooler host rock, resulting in quench times that are proportional to the vein half-thickness squared (Langenhorst and Poirier 2000; De Carli et al. 2001; Sharp et al. 2003; De Carli et al. 2003). Therefore, thin melt veins quench much faster than thicker veins and record shorter crystallization histories. For a shock event with long pulse duration, melt-vein quench, especially for narrower melt veins with a shorter quench time, should crystallize at the equilibrium shock pressure (Fig. 7). However, our study of thin veins in Tenham shows that their mineralogy does not always reflect the equilibrium pressure inferred from the thick melt veins. We observe silicate glass in the 5 μm wide melt vein (Fig. 6b), fine olivine crystals (Fig. 6c and 6d) in the 10 μm wide vein, and olivine, glass, ringwoodite, and majorite in the 30 μm wide vein (Figs. 6e and 6f).

There are four likely explanations for these assemblages

in thin melt veins in Tenham. The first is that the thinner veins could be injection veins that form in fractures that open during pressure release. If this were the case, such veins would have to tap the liquid contents of larger veins or melt pockets that were still liquid during or after pressure release. This is unlikely since low-pressure assemblages do not occur in the centers of large veins. A second alternative is that Tenham had multiple generations of shock veins and that the thin veins represent a lower-pressure shock event. This is also unlikely since we are observing different portions of the same continuous vein. A third explanation, one that accounts for the thinnest melt veins, is that they are likely to be most supercooled and quench to glass or metastable phases. The presence of metastable akimotoite at the margins of thick melt vein in Tenham indicates that rapid quench does produce low-pressure phases (Xie et al. 2006). The fourth explanation centers on the effect of pre-existing fractures on pressure equilibration during the period of ~60 μs after shock arrival, as discussed in a previous section. As illustrated by Fig. 8, the simple model with a flat-topped pressure pulse may be inappropriate for thin veins. Our thermal modeling calculations show that veins less than 10 μm wide solidify within ~12 μs, and veins less than 30 μm wide solidify within ~100 μs. Thus, it appears possible that thinner veins, <~30 μm wide, may crystallize at low pressures during the chaotic pressure equilibration process. These results suggest that the best melt veins for interpreting shock pressures from crystallization pressures are the thicker veins that are quenched more slowly and generally have assemblages that are consistent with published phase diagrams. These veins also record longer periods of crystallization history, which allows one to better constrain the shock pressure history.

CONCLUSIONS

Shock-induced melt veins provide a history of their crystallization that can be used to constrain shock pressures and pressure durations to which meteorites have been subjected. Based upon the assemblages observed, crystallization of shock veins can occur before pressure equilibration, during a period of equilibrated shock pressure, during pressure release, or after pressure release. This implies that not all melt veins are useful in constraining shock pressures from crystallization pressures. When an assemblage consists of high-pressure minerals and that assemblage is constant across a large melt vein or pocket, the crystallization pressure represents the equilibrium shock pressure. Therefore, thicker veins are better for interpreting the relationship between crystallization pressure and shock pressure. In the case of Tenham, the smallest veins appear to have quenched during a transient lower-pressure state before the shock pressure equilibrated. The present study indicates that the maximum pressure of melt-vein crystallization was ~25 GPa and that this was likely the equilibrium shock pressure for Tenham. Equilibrium shock pressures inferred from the mineralogy of shock-induced melt veins in highly shocked chondrites such as Tenham suggest that the pressure calibration of Stöffler et al. (1991) is too high by a factor of at least two for S6 samples. We suggest that differences in a single parameter, equilibrium shock pressure, do not account for the very real differences in metamorphism in shock stages S3 through S6. Other factors, such as shock duration, pre-shock porosity, and detailed stress-strain history probably also play a role.

Acknowledgments–We would like to thank Naotaka Tomioka and an anonymous reviewer for helpful reviews. We also thank Carlton Moore and the Center for Meteorite Studies at Arizona State University for supplying the samples. We also thank John Wheatley, Karl Weiss, Zhengquan Liu, and the Center for High Resolution Microscopy at ASU for assistance with the transmission and scanning electron microscopy. We also thank Jim Clark and Gordon Moore for assistance with the electron microprobe. P. S. D. thanks Bence Gerber and Chris Quan of Century Dynamics for supporting the use of Autodyn. We acknowledge NASA Cosmochemistry grants NAG5-7285, NAG5-9381, and NAG5-1977 for supporting this research.

Editorial Handling—Dr. Edward Scott

REFERENCES

Agee C. B., Li J., Shannon M. C., and Circone S. 1995. Pressure-temperature phase diagram for the Allende meteorite. *Journal of Geophysical Research* 100:725–740.

Sahara Y., Kubo T., and Kondo T. 2004. Phase relations of a carbonaceous chondrite at lower mantle conditions. *Physics of the Earth and Planetary Interiors* 143/144:421–432.

Ashworth J. R. 1985. Transmission electron microscopy of L-group chondrites, 1. Natural shock effects. *Earth and Planetary Science Letters* 73:17–32.

Begemann F. and Wlotzka F. 1969. Shock-induced thermal metamorphism and mechanical deformations in the Ramsdorf chondrite. *Geochimica et Cosmochimica Acta* 33:1351–1370.

Beck P., Gillet P., El Goresy A., and Mostefaoui S. 2005. Time scales of shock processes in chondritic and Martian meteorites. *Nature* 435:1071–1074.

Binns R. A., Davis R. J., and Reed S. J. B. 1969. Ringwoodite, natural $(Mg, Fe)_2SiO_4$ spinel in the Tenham meteorite. *Nature* 221:943–944.

Bischoff A. and Stöffler D. 1992. Shock metamorphism as a fundamental process in the evolution of planetary bodies: Information from meteorites. *European Journal of Mineralogy* 4: 707–755.

Bowden K. E. 2002. Effects of loading path on the shock metamorphism of porous quartz: An experimental study. Ph.D. thesis. University College London, London, England.

Carter N. L., Raleigh C. B., and De Carli P. S. 1968. Deformation of olivine in stony meteorites. *Journal of Geophysical Research* 73: 5439–5461.

Chao E. C. T. 1967. Shock effects in certain rock-forming minerals. *Science* 156:192–202.

Chao E. C. T. 1968. Pressure and temperature history of impact metamorphosed rocks based on petrographic observations. In *Shock metamorphism of nature materials*, edited by French B. M. and Short N. M. Baltimore, Maryland: Mono Book Corp. pp. 135–158.

Chao E. C. T., Fahey J. J., Littler J., and Milton D. J. 1962. Stishovite, SiO_2, a very high-pressure new mineral from Meteor Crater, Arizona. *Journal of Geophysical Research* 67:419–421.

Chao E. C. T., Shoemaker E. M., and Madsen B. M. 1960. First natural occurrence of coesite. *Science* 132:220–222.

Chen M., Shu J. F., Xie X. D., and Mao H. K. 2003. Natural $CaTi_2O_4$-structured $FeCr_2O_4$ polymorph in the Suizhou meteorite and its significance in mantle mineralogy. *Geochimica et Cosmochimica Acta* 67:3937–3942.

Chen M., Xie X., and El Goresy A. 2004a. A shock-produced (Mg, Fe)SiO_3 glass in the Suizhou meteorite. *Meteoritics & Planetary Science* 39:1797–1808.

Chen M., El Goresy A., Frost D., and Gillet P. 2004b. Melting experiments of a chondritic meteorite between 16 and 25 GPa: Implication for Na/K fractionation in a primitive chondritic Earth's mantle. *European Journal of Mineralogy* 16:203–211.

Chen M., Sharp T. G., El Goresy A., Wopenka B., and Xie X. 1996. The majorite-pyrope + magnesiowüstite assemblage: Constraints on the history of shock veins in chondrites. *Science* 271:1570–1573.

Cordier P. and Gratz A. J. 1995. TEM study of shock metamorphism in quartz from Sedan nuclear test site. *Earth and Planetary Science Letters* 129:163–170.

De Carli P. S. 1968. Observations of the effects of explosive shock on crystalline solids. In *Shock metamorphism of nature materials*, edited by French B. M. and Short N. M. Baltimore, Maryland: Mono Book Corp. pp. 129–134.

De Carli P. S., Aramovich C. J., Xie Z., and Sharp T. G. 2003. Meteorite studies illuminate phase transition behavior of minerals under shock compression. In *Shock compression of condensed matter—2003*, edited by Furnish M. D, Gupta Y. M., and Forbes J. W. Melville, New York: American Institute of Physics. pp. 1427–1430.

De Carli P. S., Bowden E., Sharp T. G., Jones A. P., and Price G. D. 2001. Evidence for kinetic effects on shock wave metamorphism: Laboratory experiments compared with inferences from studies of natural impact craters (abstract #1822). 32nd Lunar and Planetary Science Conference. CD-ROM.

De Carli P. S., Bowden E., Sharp T. G., Jones A. P., and Price G. D. 2002. Evidence for kinetic effects on shock wave propagation in tectosilicates. *Shock compression of condensed matter—2001*, edited by Furnish M. D, Gupta Y. M., and Forbes J. W. Melville, New York: American Institute of Physics. pp. 1381–1384.

Dodd R. T. and Jarosewich E. 1979. Incipient melting in and shock classification of L-group chondrites. *Earth and Planetary Science Letters* 44:335–340.

El Goresy A., Dubrovinsky L., Sharp T. G., Saxena S. K., and Chen M. 2000. A monoclinic polymorph of silica in the Shergotty meteorite. *Science* 288:37–55.

Fredriksson K., De Carli P. S., and Aaramäe A. 1963. Shock-induced veins in chondrites. Proceedings, Third International Space Science Symposium. pp. 974–983.

Gasparik T. 1992. Melting experiments on the enstatite-pyrope join at 80–152 kbar. *Journal of Geophysical Research* 97:15,181–15,188.

Gault D. E., Quaide W. L., and Oberbeck V. R. 1968. Impact cratering mechanics and structures. In *Shock metamorphism of nature materials*, edited by French B. M. and Short N. M. Baltimore, Maryland: Mono Book Corp. pp. 87–100.

Gillet P., Chen M., Dubrovinsky L., and El Goresy A. 2000. Natural $NaAlSi_3O_8$-hollandite in the shocked Sixiangkou meteorite. *Science* 287:1633–1636.

Goltrant O., Cordier P., and Doukhan J.-C. 1991. Planar deformation features in shocked quartz: A transmission electron microscopy investigation. *Earth and Planetary Science Letters* 106:103–115.

Goltrant O., Leroux H., Doukhan J.-C., and Cordier P. 1992. Formation mechanisms of planar deformation features in naturally shocked quartz. *Physics of the Earth and Planetary Interiors* 74:219–240.

Grady D. E., Murri W. J., and De Carli P. S. 1975. Hugoniot sound velocities and phase transformations in two silicates. *Journal of Geophysical Research* 80:4857–4861.

Heymann D. 1967. On the origin of hypersthene chondrites: Ages and shock effects of black chondrites. *Icarus* 6:189–221.

Kenkmann T., Hornemann U., and Stöffler D. 2000. Experimental generation of shock-induced pseudotachylites along lithological interfaces. *Meteoritics & Planetary Science* 35:1275–1290.

Kieffer S. W. 1971. Shock metamorphism of the Coconino sandstone at Meteor Crater, Arizona. *Journal of Geophysical Research* 76: 5449–5473.

Kieffer S. W. 1975. From regolith to rock by shock. *The Moon* 13: 301–320.

Langenhorst F., Joreau P., and Doukhan J. C. 1995. Thermal and shock metamorphism of the Tenham chondrite: A TEM examination. *Geochimica et Cosmochimica Acta* 59:1835–1845.

Langenhorst F. and Poirier J. P. 2000. Anatomy of black veins in Zagami: Clues to the formation of high-pressure phase. *Earth and Planetary Science Letters* 184:37–55.

Leroux H. 2001. Microstructural shock signatures of major minerals in meteorites. *European Journal of Mineralogy* 13:253–272.

Mason B., Nelen J., and White J. S., Jr. 1968. Olivine-garnet transformation in a meteorite. *Science* 160:66–67.

Melosh H. J. 1989. *Impact cratering: A geologic process*. New York: Oxford University Press. 245 p.

Milton D. J. and De Carli P. S. 1963. Maskelynite: Formation by explosive shock. *Science* 140:670–671.

Nesterenko V. F. 2001. *Dynamics of heterogeneous materials*. New York: Springer-Verlag. 510 p.

Oguri K., Funamori N., Sakai F., Kondo T., Uchida T., and Yagi T. 1997. High-pressure and high-temperature phase transitions in diopside $CaMgSi_2O_6$. *Physics of the Earth and Planetary Interiors* 104:363–370.

Price G. D., Putnis A., and Agrell S. O. 1979. Electron petrography of shock-produced veins in the Tenham chondrite. *Contributions to Mineralogy and Petrology* 71:211–218.

Price G. D., Putnis A., and Smith D. G. W. 1982. A spinel to ß-phase transformation mechanism in $(Mg,Fe)_2SiO_4$. *Nature* 296:729–731.

Putnis A. and Price G. D. 1979. High-pressure $(Mg, Fe)_2SiO_4$ phases in the Tenham chondritic meteorite. *Nature* 280:217–218.

Reichenbach F. v. 1860. I. Meteoriten in Meteoriten. *Annalen der Physik und Chemie* 187:353–386.

Schmitt R. T. 2000. Shock experiments with the H6 chondrite Kernouvé: Pressure calibration of microscopic shock effects. *Meteoritics & Planetary Science* 35:545–560.

Sharp T. G. and De Carli P. S. 2006. Shock effects in meteorites. In *Meteorites and the early solar system II*, edited by Lauretta D. S. and McSween H. Y., Jr. Tucson, Arizona: The University of Arizona Press. pp. 653–677.

Sharp T. G., El Goresy A., Wopenka B., and Chen M. 1999. A post-stishovite SiO_2 polymorph in the meteorite Shergotty: Implications for impact events. *Science* 284:1511–1513.

Sharp T. G., Lingemann C. M., Dupas C., and Stöffler D. 1997. Natural

occurrence of $MgSiO_3$-ilmenite and evidence for $MgSiO_3$-perovskite in a shocked L chondrite. *Science* 277:352–355.

Sharp T. G., Xie Z., Aramovich C. J., and De Carli P. S. 2003. Pressure-temperature histories of shock-induced melt veins in chondrites (abstract #1278). 34th Lunar and planetary science conference. CD-ROM.

Shoemaker E. M. and Chao E. C. T. 1961. New evidence for the impact origin of the Ries Basin, Bavaria, Germany. *Journal of Geophysical Research* 66:3371–3378.

Spray J. G. 1998. Localized shock- and friction-induced melting in response to hypervelocity impact. In *Meteorites: Flux with time and impact effects*, edited by Grady M. M., Hutchison R., McCall G. J. H., and Rotherby D. A. London: Geological Society. pp. 171–180.

Stöffler D. 1972. Deformation and transformation of rock-forming minerals by natural and experimental shock processes: I. Behavior of minerals under shock compression. *Fortschritte der Mineralogie* 49:50–113.

Stöffler D. 1974. Deformation and transformation of rock-forming minerals by natural and experimental shock processes: II. Physical properties of shocked minerals. *Fortschritte der Mineralogie* 51:256–289.

Stöffler D., Keil K., and Scott E. R. D. 1991. Shock metamorphism of ordinary chondrites. *Geochimica et Cosmochimica Acta* 55: 3845–3867.

Taylor G. J. and Heymann D. 1969. Shock, reheating, and the gas retention ages of chondrites. *Earth and Planetary Science Letters* 7:151–161.

Thompson A. B. and Tracy R. J. 1979. Model systems for anatexis of pelitic rocks II. Facies series melting and reactions in the system CaO-$KAlO_2$-$NaAlO_2$-AlO_3-SiO_2-H_2O. *Contributions to Mineralogy and Petrology* 70:429–438.

Tomeoka K., Yamahana Y., and Sekine T. 1999. Experimental shock metamorphism of the Murchison CM carbonaceous chondrite. *Geochimica et Cosmochimica Acta* 63:3683–3703.

Tomioka N. and Fujino K. 1997. Natural $(Mg,Fe)SiO_3$-ilmenite and -perovskite in the Tenham meteorite. *Science* 277:1084–1086.

Van Schmus W. R. and Ribbe P. H. 1968. The composition and structural state of feldspar from chondritic meteorites. *Geochimica et Cosmochimica Acta* 32:1327–1342.

Van Schmus W. R. and Wood J. A. 1967. A chemical-petrologic classification for the chondritic meteorites. *Geochimica et Cosmochimica Acta* 31:747–765.

Xie Z. and Sharp T. G. 2000. Mineralogy of shock-induced melt veins in chondrites as a function of shock grade (abstract #2065). 31st Lunar and Planetary Science Conference. CD-ROM.

Xie Z. and Sharp T. G. 2004. High-pressure phases in shock-induced melt veins of the Umbarger L6 chondrite: Constraints on shock pressure. *Meteoritics & Planetary Science* 39:2043–2054.

Xie Z., Sharp T. G., and De Carli P. S. 2006. High-pressure phases in a shock-induced melt vein of Tenham L6 chondrite: Constraints on shock pressure and duration. *Geochimica et Cosmochimica Acta* 70:504–515.

Xie Z., Tomioka N., and Sharp T. G. 2002. Natural occurrence of Fe_2SiO_4-spinel in the shocked Umbarger L6 chondrite. *American Mineralogist* 87:1257–1260.

Yamaguchi A., Scott E. R. D., and Keil K. 1996. Petrology of unique impact melt rock, Ramsdorf (L chondrite). 27th Lunar and Planetary Science Conference. pp. 1467–1468.

Zhang J. and Herzberg C. 1994. Melting experiments on anhydrous peridotite KLB-1 from 5.0 to 22.5 GPa. *Journal of Geophysical Research* 99:17,729–17,742.